Modulated point-vortex couples on a beta-plane: dynamics and chaotic advection

I. J. BENCZIK[1]†, T. TÉL[2] AND Z. KÖLLŐ[2]

[1]Max Planck Institute for the Physics of Complex Systems, Dresden, Germany

[2]Institute for Theoretical Physics, Eötvös University, PO Box 32, H-1518 Budapest, Hungary

The dynamics of modulated point-vortex couples on a β-plane is investigated for arbitrary ratios of the vortex strength. The motion is analysed in terms of an angle- and a location-dependent potential and the structural changes in their shape. The location-dependent potential is best suited for understanding different types of vortex orbits. It is shown to be two-valued in a range of parameters, a feature which leads to the appearance of orbits with spikes, in spite of the integrability of the problem. The advection dynamics in this modulated two-vortex problem is chaotic. We find a transition from closed to open chaotic advection, implying that the transport properties of the flow might be drastically altered by changing some parameters or the initial conditions. The open case, characterized by permanent entrainment and detrainment of particles around the vortices, is interpreted in terms of an invariant chaotic saddle of the Lagrangian dynamics, while the dynamics of the closed case, with a permanently trapped area of the fluid, is governed by a chaotic region and interwoven KAM tori. The transition from open to closed chaotic advection is quantified by monitoring the escape rate of advected particles as a function of the vortex energy.

1. Introduction

The presence of gradients in the background vorticity makes the dynamics – even of point vortices (see e.g. Newton 2001) – surprisingly non-trivial, and the advection chaotic. Much interest comes from the geophysical fluid dynamics community since such a gradient appears due to the variation of the Coriolis parameter with the latitudinal coordinate, which is referred to as the 'beta-effect' (Pedlosky 1979).

In the simplest case of a homogeneous, incompressible, two-dimensional, and ideal fluid, the potential vorticity (Pedlosky 1979), $q \equiv \zeta + \beta' y$, is conserved by each particle along its trajectory, where ζ is the relative vorticity, y the latitudinal coordinate, and β' the beta parameter.

As pointed out by Makino, Kamimura & Taniuti (1981), Zabusky & McWilliams (1982), Hobson (1991) and Velasco Fuentes & van Heijst (1994), the principle of the conservation of potential vorticity can be introduced into the point-vortex picture by applying a modulation of the vortex strength with the latitudinal coordinate. The strength $\kappa_i(y)$ of any vortex i therefore fulfils $\kappa_i(y) + \beta y = \text{const}$, from which

$$\kappa_i(y) = \kappa_{i0} - \beta y, \tag{1.1}$$

† Present address: Physics Department, Virginia Tech, Blacksburg, VA 24061, USA.

where κ_{i0} is the vortex strength at $y = 0$. Parameter β is the analogue of β'.† Since κ is a circulation, the dimension of β is area times that of β'. The vortex strength thus decreases when moving towards the north (y grows). By applying (1.1), we neglect the vorticity production due to the transport of fluid elements outside the vortices, as discussed by Velasco Fuentes & van Heijst (1994). The modulated point-vortex model is therefore valid as long as this vorticity gain is negligible.

Although such point vortices are not exact solutions of the hydrodynamical equations, they have been shown to be useful in understanding several properties of the quasigeostrophic equation, such as the existence of modon-like excitations (Makino *et al.* 1981). Later, Velasco Fuentes, van Heijst and collaborators pointed out that laboratory-generated vortices on a topographic β-plane (sloping bottom) could be approximated quite well by the modulated point-vortex model over a considerable time span. These investigations were carried out for a pair of nearly dipolar vortices (Kloosterziel *et al.* 1993; Velasco Fuentes & van Heijst 1994; Velasco Fuentes *et al.* 1995) and nearly identical vortices (Velasco Fuentes & Velázques Mũnoz 2003). The modulated point-vortex approach provides vortex couple orbits which are qualitatively similar to those obtained from a recent exact treatment of point vortices on a rotating sphere (Newton & Shokraneh 2006; Jamalooden & Newton 2006).

One of the aims of this paper is to provide a systematic exploration of the dynamics for a wide range of strength ratios in the two-vortex problem. To this end, we introduce a new potential depending on the latitudinal coordinate, but we also use an angle-dependent potential already suggested for a special case in Velasco Fuentes & Velázques Mũnoz (2003), and show that qualitative changes in the vortex dynamics follow as bifurcation-like events in the shapes of these potentials. In certain ranges of parameters, the potential depending on the latitudinal coordinate has the unusual feature of being bi-valued. The change from one branch to the other leads to a point of non-differentiability in the orbit. The region of parameter space in which none of the vortices can change sign during their entire motion is determined.

The second aim of the paper is to analyse the material transport in the field of the two modulated point vortices. The first step towards understanding the passive advection dynamics (Aref 1984; Ottino 1989; Aref 2002) has been made by Velasco Fuentes & van Heijst (1994) for dipolar vortices, but recent advancement in the theory of chaotic advection suggest that a detailed reinvestigation is warranted. In particular, for nearly dipolar cases the flow in the frame co-moving with the vortex centres can be considered to be open (Jung, Tél & Ziemniak 1993; Péntek, Tél & Toroczkai 1995; Sommerer, Ku & Gilreath 1996), which implies that particles are trapped by the vortices for a finite time only, and eventually all advected particles leave the wake. There is an infinite set of unstable, never escaping orbits – the so-called chaotic saddle (Jung *et al.* 1993; Péntek *et al.* 1995) – which is, however, a set of zero area, a fractal. This set is responsible for the permanent entrainment and detrainment process of tracer particles described by Velasco Fuentes *et al.* (1995). By changing either the vortex strength or the initial position of the couple, we show that this process stops and one can always find a transition to a closed flow regime, where chaotically advected particles remain around the vortices for arbitrarily long times.

---

† Another equivalent parameterization of the modulation is $\kappa_i(y) = \kappa_{i0}^* - \beta(y - y_{i0})$, where κ_{i0}^* is the vortex strength at the initial position y_{i0} (see e.g. Kloosterziel, Carnevale & Philippe 1993 and Velasco Fuentes, van Heijst & Cremers 1995). For mathematical convenience we use parameterization (1.1) since the analogy with classical mechanics, worked out in §3, is cleanest with this form.

Thus, a mere change in the initial conditions can result in a drastic change in the transport properties of the couple.

In §2 we write the equations for a point vortex couple on the β-plane. An angle-dependent and a location-dependent potential is shown in §3 to govern the dynamics, which undergo several bifurcations as the parameters are changed. Conditions for sign-changing of the vortices are derived in §4. Sections 5 and 6 are devoted to the description of the dynamics of significantly different and of similar vortex couples, respectively, in which the vortex strengths never change sign. Other cases are briefly discussed in §7. In the Appendix a perturbative analytical condition is derived for the figure-of-eight-shaped orbit. Section 8 is devoted to the advection dynamics. The chaotic sets and droplet patterns are investigated both in the closed and open advection regime. The strength of openness is characterized by the escape rate determined as a function of the vortex energy. In the concluding §9, we summarize our findings and point out an interesting analogy with the dynamics of a point mass on a rotating sphere (Paldor & Killworth 1988; Paldor & Boss 1992; Dvorkin & Paldor 1999; Paldor 2007).

2. The model

We consider two-dimensional point vortices in a Cartesian coordinate system where x represents the longitude and y the latitude. The strength of vortex i at an arbitrary y is assumed to be given by (1.1).

The equations of motion for N interacting vortices centred at (x_i, y_i) are (see e.g. Newton 2001)

$$\frac{\mathrm{d}x_i}{\mathrm{d}t} = -\sum_{j=1, j\neq i}^{N} \frac{\kappa_j(y_j)(y_i - y_j)}{r_{ij}^2}, \qquad \frac{\mathrm{d}y_i}{\mathrm{d}t} = \sum_{j=1, j\neq i}^{N} \frac{\kappa_j(y_j)(x_i - x_j)}{r_{ij}^2}, \qquad (2.1)$$

where $i, j = 1, \ldots, N$, and

$$r_{ij} = \sqrt{(x_i - x_j)^2 + (y_i - y_j)^2} \qquad (2.2)$$

denotes the distance between vortices i and j.

By writing the explicit y-dependence of the vortex strengths, for two vortices ($N = 2$) (2.1) becomes

$$\frac{\mathrm{d}x_i}{\mathrm{d}t} = -\frac{(\kappa_{i+1,0} - \beta y_{i+1})(y_i - y_{i+1})}{r_{12}^2}, \qquad \frac{\mathrm{d}y_i}{\mathrm{d}t} = \frac{(\kappa_{i+1,0} - \beta y_{i+1})(x_i - x_{i+1})}{r_{12}^2}, \qquad (2.3)$$

with $i = 1, 2 \mod (2)$. The vortex distance r_{12} turns out to be a constant of the motion, which is denoted by D.

We shall see that the dynamics is qualitatively different for the parameter combination

$$\sigma = \frac{|\kappa_{10} - \kappa_{20}|}{\beta D} \qquad (2.4)$$

lying above or below unity. We call these cases significantly different or similar vortices, respectively.

The equations of motion can be cast into a dimensionless form by measuring distance in units of D and vortex strength in units of κ_{10}, which we assume to be positive. As a consequence, the time unit is D^2/κ_{10}. In these units, the dimensionless

equations of motion are

$$\frac{dx_1}{dt} = -(\kappa - \beta y_2)(y_1 - y_2), \quad \frac{dy_1}{dt} = (\kappa - \beta y_2)(x_1 - x_2), \tag{2.5}$$

$$\frac{dx_2}{dt} = -(1 - \beta y_1)(y_2 - y_1), \quad \frac{dy_2}{dt} = (1 - \beta y_1)(x_2 - x_1), \tag{2.6}$$

where $\kappa \equiv \kappa_{20}/\kappa_{10}$, and β represents the dimensionless beta-parameter expressed as $\beta D/\kappa_{10}$ in the original variables. We always choose vortex 1 to be the stronger, and therefore $|\kappa| < 1$. The dimensionless form of parameter σ is consequently

$$\sigma = \frac{1 - \kappa}{\beta}. \tag{2.7}$$

Now we introduce relative and 'centre of mass' coordinates as

$$x_r = x_2 - x_1, \quad y_r = y_2 - y_1, \tag{2.8}$$

$$x = \frac{x_1 + x_2}{2}, \quad \bar{y} = \frac{y_1 + y_2}{2}. \tag{2.9}$$

The conservation of vortex distance implies: $x_r^2 + y_r^2 = 1$. The differential equations for the relative coordinates follow from (2.5) and (2.6) as

$$\frac{1}{\beta}\frac{dx_r}{dt} = 2yy_r, \quad \frac{1}{\beta}\frac{dy_r}{dt} = -2yx_r. \tag{2.10}$$

Here

$$y \equiv \bar{y} - \sigma'/2 \tag{2.11}$$

is a shifted centre-of-mass coordinate, and

$$\sigma' = \frac{1 + \kappa}{\beta}. \tag{2.12}$$

The equations of the centre-of-mass coordinates are obtained in a similar fashion as

$$\frac{1}{\beta}\frac{dx}{dt} = -\frac{(\sigma + y_r)y_r}{2}, \quad \frac{1}{\beta}\frac{dy}{dt} = \frac{(\sigma + y_r)x_r}{2}. \tag{2.13}$$

These equations indicate that by considering σ to be the basic parameter of the model, the dimensionless parameter β is merely a scale factor of time.† When varying parameter σ, we have to keep in mind that in order be able to neglect the vorticity generated by the ambient fluid, β should be kept small (Velasco Fuentes & van Heijst 1994). This constraint, however, does, not influence the accessible range of σ as $(0, \infty)$.

3. Potentials

Besides the vortex distance, the energy of rotation turns out to be another constant of the motion. Let α be the angle between the y-axis and the line joining the vortices (see figure 1):

$$\sin\alpha = x_r, \quad \cos\alpha = -y_r. \tag{3.1}$$

† With parameterization $\kappa_i(y) = \kappa_{i0}^* - \beta(y - y_{i0})$, one also recovers (2.10)–(2.13) but the dimensionless parameters σ and σ' are then replaced by $\sigma^* = (1-\kappa)/\beta - y_{r0}$ and $\sigma^{*'} = (1+\kappa)/\beta + y_0$, respectively. It is the appearance of the initial coordinates in σ^* and $\sigma^{*'}$ which makes this parameterization inconvenient for the potential picture.
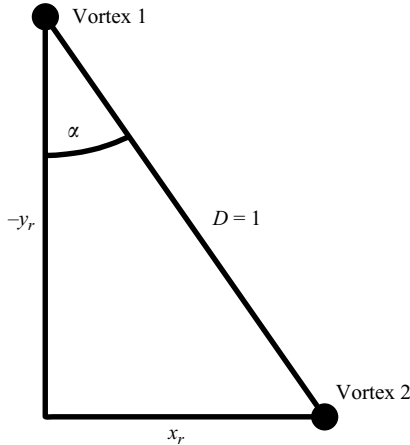
FIGURE 1. The rotational angle α in terms of the relative vortex coordinates. In this diagram, $\alpha > 0$, in general $-\pi \leqslant \alpha \leqslant \pi$.

From (2.10) we obtain

$$\frac{1}{\beta}\frac{\mathrm{d}\alpha}{\mathrm{d}t} = -2y \tag{3.2}$$

which implies that the centre-of-mass coordinate $\bar{y}$, or rather its shifted value y, uniquely determines the instantaneous angular velocity of the line connecting the vortices.

By taking the time derivative of (3.2) and substituting (2.13) and (3.1), one finds

$$\frac{1}{\beta^2}\frac{\mathrm{d}^2\alpha}{\mathrm{d}t^2} = -\sigma \sin\alpha + \tfrac{1}{2}\sin 2\alpha \equiv -\frac{\mathrm{d}W(\alpha)}{\mathrm{d}\alpha} \tag{3.3}$$

with an angle-dependent potential:

$$W(\alpha) = -\sigma \cos\alpha + \tfrac{1}{4}\cos 2\alpha + \sigma - \tfrac{1}{4}. \tag{3.4}$$

The additive constant has been introduced to make the energy of the state $\alpha = 0$ zero. For equal vortices, $\sigma = 0$, this potential has been identified in Velasco Fuentes & Velázques Mũnoz (2003).

The rotational energy

$$E = \frac{1}{2\beta^2}\left(\frac{\mathrm{d}\alpha}{\mathrm{d}t}\right)^2 - \sigma\cos\alpha + \tfrac{1}{4}\cos 2\alpha + \sigma - \tfrac{1}{4} \tag{3.5}$$

is thus a constant of motion. In view of (3.2),

$$E = 2y^2 - \sigma\cos\alpha + \tfrac{1}{4}\cos 2\alpha + \sigma - \tfrac{1}{4}. \tag{3.6}$$

This is a relation between the centre-of-mass coordinate y and angle α at fixed energies E (see figure 2). From this, the angle can be expressed by means of y as

$$\cos\alpha = \sigma \pm F(y) \tag{3.7}$$

with

$$F(y) = \sqrt{(\sigma - 1)^2 + 2E - 4y^2}. \tag{3.8}$$

Potential W does not contain direct information about the centre-of-mass dynamics. In addition, as shown by (3.7), the relation between angle and y is not one-to-one.
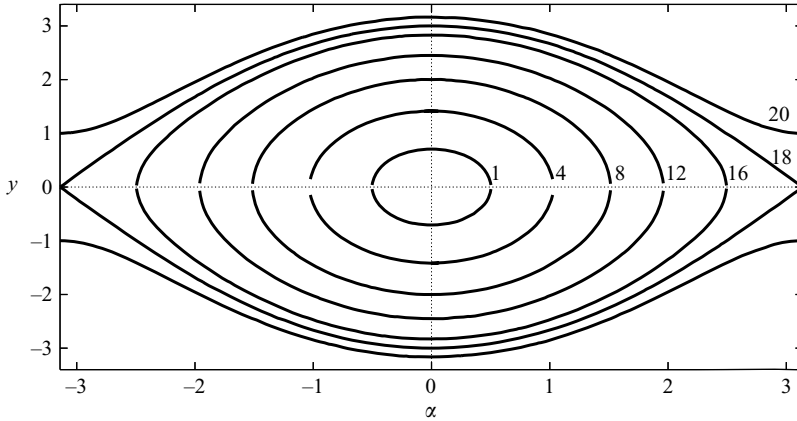
FIGURE 2. Relation between the centre-of-mass coordinate y and angle α at different rotational energies E ($\sigma = 9$). The energy values are indicated along the contours.

It is therefore important to derive a potential governing the behaviour along the y-direction. From (2.13), (3.1) and (3.7) we obtain

$$\frac{1}{2\beta^2}\left(\frac{dy}{dt}\right)^2 = \frac{F(y)^2(1 - (\sigma \pm F(y))^2)}{8}. \tag{3.9}$$

This equation is of the form $(\dot{y})^2/(2\beta^2) + V_\pm(y) = 0$ with the potential

$$V_\pm(y) = \tfrac{1}{8}F(y)^2((\sigma \pm F(y))^2 - 1). \tag{3.10}$$

The y-dynamics is thus a potential motion in $V_\pm(y)$ with *zero* total energy. Motion must therefore be restricted to intervals where $V_\pm(y) \leqslant 0$.

Potentials $W(\alpha)$ and $V_\pm(y)$ reflect two different facets of the vortex dynamics: rotation (corresponding to a kind of internal degree of freedom) and centre-of-mass motion in the north–south direction, respectively.

In expression (3.10) for the potential $V_\pm$, F appears with two signs. We therefore discuss the sign to be taken in different cases. For $\sigma > 1$, $\sigma - \cos\alpha$ is positive, and only the lower sign can be valid in (3.7); therefore, only one potential, $V_- \equiv V$ exists. For $\sigma < 1$, the sign of F can be both positive and negative. A change of sign can only occur if $F(y)$ vanishes, i.e. at the extremal values $\pm y_e$ of the potential, where

$$y_e = \tfrac{1}{2}\sqrt{(\sigma - 1)^2 + 2E}. \tag{3.11}$$

For $|y| > y_e$ expression (3.10) is complex.

These considerations show that a bifurcation of the vortex dynamics takes place at $\sigma = 1$. For $\sigma > 1$, the location-dependent potential has a single branch, and the angle-dependent potential is always single-welled, while for $\sigma < 1$ the location-dependent potential has two branches and the angle-dependent one is double-welled (as illustrated by the figures of §5 and §6). The dynamics in the two regimes is basically different; therefore we shall discuss the dynamics of significantly different vortices ($\sigma > 1$) and of similar vortices ($\sigma < 1$) separately.

The vortex motion is uniquely specified by its initial centre-of-mass location (x_0, y_0), and initial angle α_0. Owing to the translational invariance in x, the character of the dynamics does not depend on x_0. In order to exploit the properties of the potential motion, we shall investigate the behaviour of the angle and the centre-of-mass coordinate y at different energies E. In view of (3.6), changing the energy at a fixed y
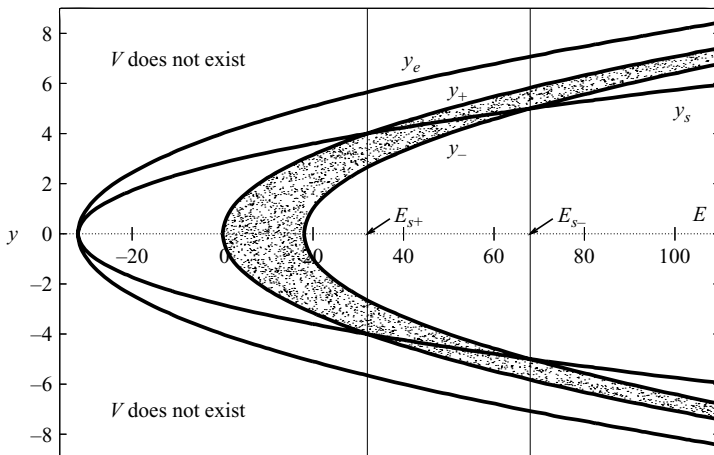
FIGURE 3. Range of y (grey) over which the centre-of-mass motion extends (i.e. $V \equiv V_- < 0$) as a function of the rotation energy, E, for significantly different vortices ($\sigma = 9$). In order to avoid sign changing of the vortex strength, the energy must be either $E < E_{s+}$ or $E > E_{s-}$. The characteristic points y_e, y_s, and $y_\pm$ are also indicated as functions of energy.

(or fixed α) implies choosing another initial angle α_0 (or initial y_0), as demonstrated by figure 2.

4. Conditions for sign changes of vortex strengths

In the context of vortices on the rotating Earth or of experiments, a sign change of any of the vortices in the course of their motion is unrealistic. To see under which conditions this happens in the model, we determine here the energies at which the vortices change their signs. Using (2.8), (2.9) and (3.7), the dimensionless vortex strengths $\kappa_1(y_1)/\kappa_{10}$ and $\kappa_2(y_2)/\kappa_{10}$ can be expressed by the centre of mass coordinate as $(\beta/2)(\pm F(y) - 2y)$ and $(\beta/2)(\mp F(y) - 2y)$, respectively. From these equations the 'sign-changing y-coordinates' are $\pm y_s$, where

$$y_s = \sqrt{\frac{(\sigma - 1)^2 + 2E}{8}} = \frac{y_e}{\sqrt{2}} \qquad (4.1)$$

is the positive solution of $F(y) = 2y$. Since a more positive vortex reaches the sign-changing configuration at a larger distance (remember κ_{10} is positive), y_s and $-y_s$ correspond to the sign-changing coordinates of vortex 1 and vortex 2, respectively (cf. figures 3 and 4). If potential $V_\pm$ allows motion across these points, the sign of one of the vortices changes.

The motion occurs on y-intervals which fall between the zeros of $V(y)$ (see (3.10)): $\pm y_e$ and $\pm y_\pm$, where

$$y_\pm = \tfrac{1}{2}\sqrt{\pm 2\sigma - 2\sigma + 2E}. \qquad (4.2)$$

The characteristic point y_+ and y_- vanishes for $E = 0$ and $E = 2\sigma$, respectively (cf. figures 3 and 4).

For $\sigma > 1$, motion occurs for $E > 0$ (see figure 3). This follows from the fact that the minimum of potential (3.4) is zero. Motion is restricted to the interval $(-y_+, y_+)$ for $0 < E < 2\sigma$ (since y_- is then imaginary), and to the intervals $\pm(y_-, y_+)$ for $E > 2\sigma$ (see the shaded region of figure 3). In order to avoid sign changing of any of the two
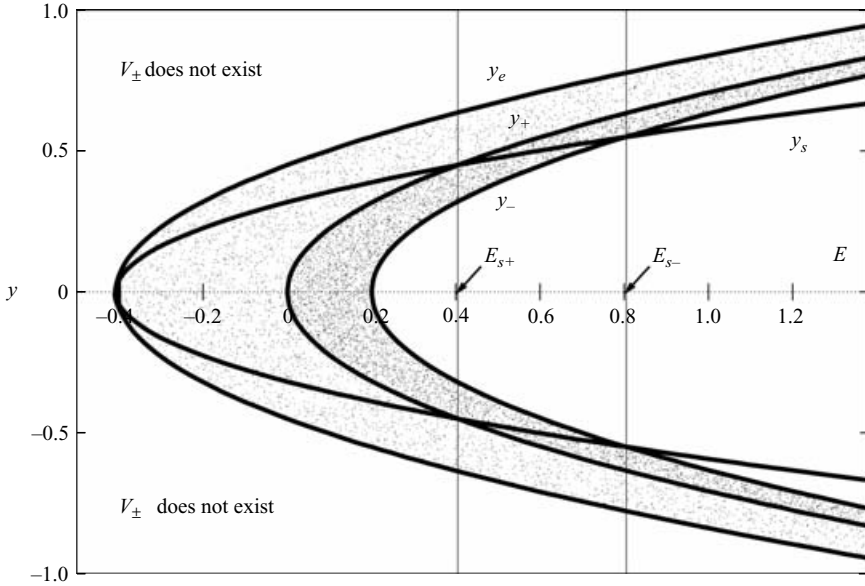
FIGURE 4. As figure 3 but for similar vortices ($\sigma = 0.1$). The location-dependent potential is bi-valued: both V_+ and V_- exist, cf. (3.10). Motion in V_+ ($V_+ < 0$) is limited to the light grey region between y_e and y_+, while motion in V_- is possible ($V_- < 0$) in the entire shaded region.

vortices, y_s must be outside the y interval in which motion takes place. The energy of the system must then be

$$\text{either} \quad E < E_{s+} \quad \text{or} \quad E > E_{s-}, \tag{4.3}$$

where

$$E_{s\pm} = \tfrac{1}{2}(\sigma + 1)^2 \mp 2\sigma \tag{4.4}$$

denotes the energies for which $y_\pm = y_s$. It is easy to check that both vortices are of the same sign for $E > E_{s-}$ (positive for $y < 0$). They are of opposite sign for $E < E_{s+}$. A detailed investigation of the dynamics in the range of (4.3) will be given in §5.

For $\sigma < 1$, both branches of potential (3.10) exist, and V_- has the same expression as in the case of significantly different vortices. Functions $V_+(y)$ and $V_-(y)$ change sign for y_+ and y_-, respectively. Thus the motion is restricted to $(-y_e, y_e)$ for energies $E_{min} < E < 2\sigma$, and to $\pm(y_-, y_e)$ for energies $E > 2\sigma$ (see figure 4). The minimum energy $E_{min} = -(\sigma - 1)^2/2$ for which motion can occur is determined by the condition $y_e = 0$. Sign changing of the vortex strength can only be avoided for

$$E > E_{s-} \tag{4.5}$$

(see figure 4), where both vortices have the same sign. The dynamics in this range will be discussed in §6.

For mathematical completeness, a brief discussion of the dynamics of sign-changing vortices will be given in §7. We note, however, that even in the case of unchanged signs, the total dimensionless vortex strength $(\kappa_1(y_1) + \kappa_2(y_2))/\kappa_{10} = -2\beta y$ changes its sign at the symmetry centre of potential $V_\pm$.
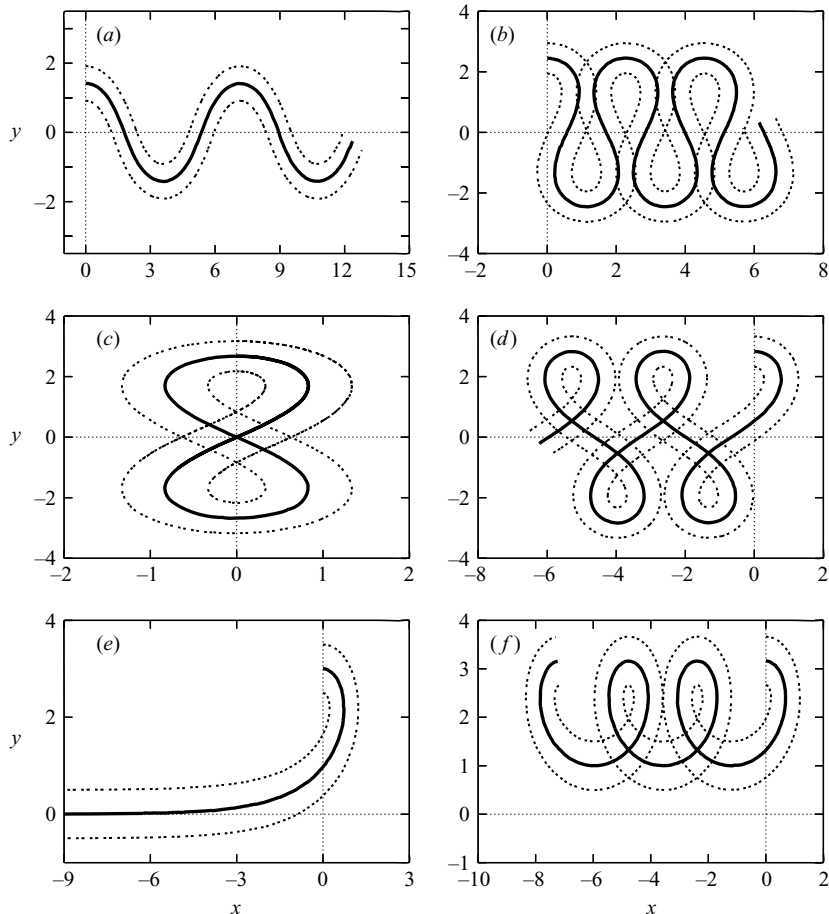
FIGURE 5. Vortex dynamics on the (x, y)-plane at various energies. The dashed and continuous lines represent the orbits of vortices and the centre of mass, respectively. Initial conditions: $\alpha_0 = 0$ $y_0 = \sqrt{E/2}$ (as follows from the energy conservation (3.6)). Parameters: $\sigma = 9, \sigma' = 1$ ($\kappa = -0.8, \beta = 0.2$), and the energies are (a) $E = 4$, (b) $E = 12$, (c) $E = E_8 = 14.274612$, (d) $E = 16$, (e) $E = 18$, and (f) $E = 20$. The duration of simulation is, from (a) to (f), $t_{sim} = 15, 25, 40, 40$ and 25 dimensionless time units, respectively.

5. Dynamics of significantly different vortices: $\sigma > 1$

For $E = 0$, only a single angle $\alpha = 0$ can occur, and from (3.6), $y = 0$. The two vortices are of opposite strength and the couple moves as a vortex pair (a 'modon') along a straight line to the right.

At small positive energy values, the vortices (forming a 'tilted modon' (Velasco Fuentes & van Heijst 1994)) carry out a weakly meandering motion (figure 5a). The orbits are periodic in x, and their average velocity is positive in the x-direction.

At $E = \sigma - 1/2$ the orbit starts 'turning back': the vortices travel parallel to the y-direction for a moment. It is at this energy (see the continuous line in figure 6) that the angles $\alpha = \pm\pi/2$ become first accessible.

For $E > \sigma - 1/2$ the orbits are 'strongly' meandering (figure 5b): the vortices turn in the negative x-direction for a while, but the net x-velocity is still positive. By further increasing the energy, the average velocity vanishes at a certain energy E_8, (figure 5c),
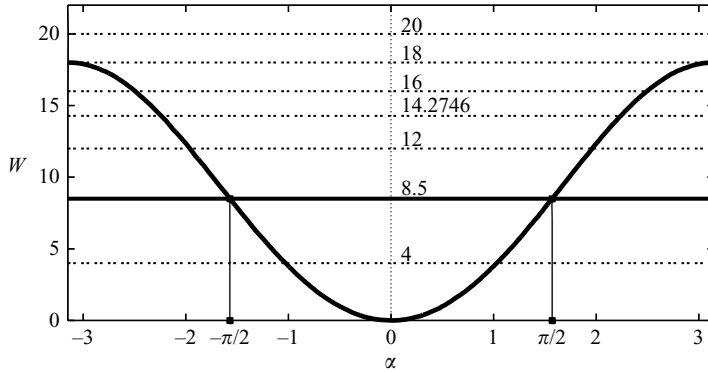
FIGURE 6. The angle-dependent potential $W(\alpha)$ ($\sigma = 9$). The energies used in figure 5 are indicated as dashed horizontal lines. The continuous horizontal line is $E = \sigma - \frac{1}{2}$, where 'turning back' first appears.

and the orbit becomes a figure-of-eight-shaped closed loop. For $E > E_8$ the vortices begin to drift in the negative x-direction (figure 5d). The orbits cross themselves, and are of cycloid type, but the motion is periodic again with an increasing wavelength.

At a certain energy E_c the wavelength becomes infinite, the centre of mass cannot cross the $y = 0$ level, and the y-coordinate approaches that level asymptotically. The vortex angle converges towards $\alpha = -\pi$. As we can see from figure 5(e), the motion is aperiodic and is no longer symmetric around $y = 0$.

At higher energies the orbits are asymmetric, but periodic again (figure 5f). The motion is a looping around a point that moves to the left. One can see that the centre of mass is always above the $y = 0$ level in figure 5(f).

We note that potential $W(\alpha)$ provides information on the rotational dynamics only. It is clear that the critical energy

$$E_c = 2\sigma \tag{5.1}$$

is the maximum energy of $W(\alpha)$ at the unstable point $\alpha = \pm\pi$ (see figure 6). In view of (3.2), $y = -(1/2\beta)\mathrm{d}\alpha/\mathrm{d}t$, the pattern of the (α, y)-plane shown in figure 2 corresponds therefore to that of the phase plane $(\alpha, \mathrm{d}\alpha/\mathrm{d}t)$. The trajectory at the critical energy is a separatrix between the symmetric and asymmetric motion. Below E_c, the angle changes periodically in a finite interval (libration), while above the critical value, the vortices rotate in one direction permanently (overturning).

The location-dependent potential $V(y)$ given by (3.10) provides direct insight into the shape of orbits. For small energies the orbits are sine-like oscillations around the minimum at $y = 0$ (see figure 7a). As the rotational energy increases, a local maximum in V develops around $y = 0$, where the y-velocity decreases. As long as the potential hill is small, the vortices turn back in the negative x-direction for a while (figure 7b), but above E_8 the hill is so high that an overall drift develops in the negative x-direction (figure 7d). Note that at E_8 (figure 7c) no specific change occurs in $V(y)$: the appearance of the figure-of-eight orbit is due to an interplay between the y- and the x-dynamics (see the Appendix).

At the critical E_c the central hill touches the y-axis from below (figure 7e), then extends beyond the y-axis and prevents the centre of mass from approaching the $y = 0$ line (figure 7f). This critical energy value therefore marks the onset of spontaneous symmetry breaking for the orbits.
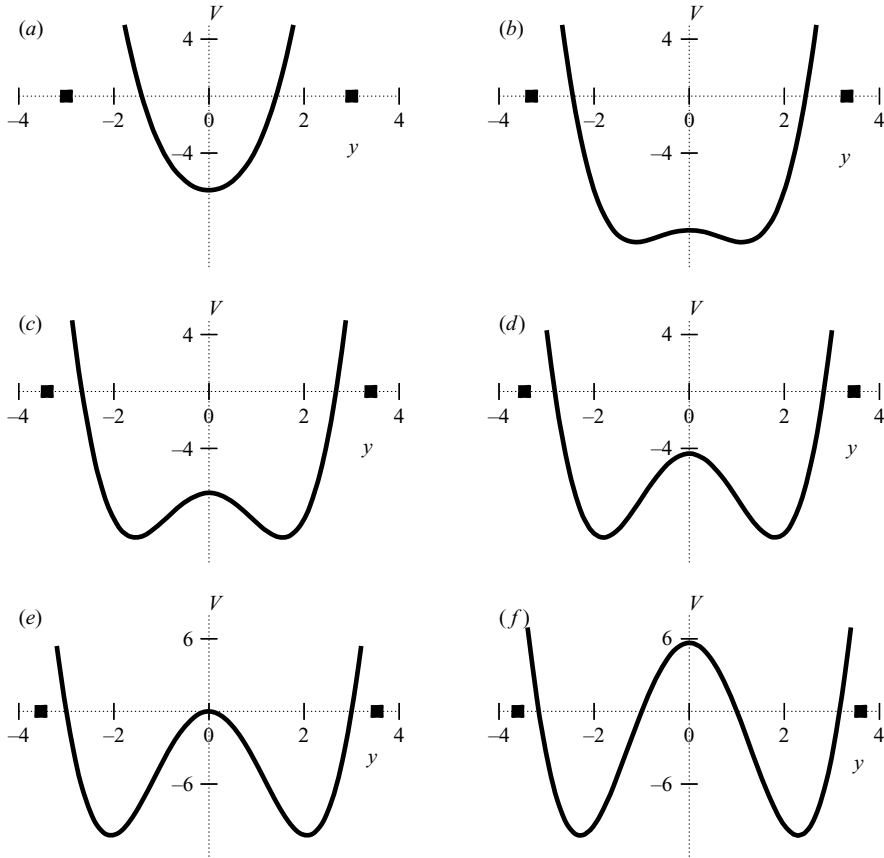
FIGURE 7. The location-dependent potential $V(y)$ corresponding to the dynamics shown in figure 5. The characteristic points $\pm y_s$ determined by (4.1) are denoted by filled squares. They fall outside of the accessible region so that the vortices do not change sign.

6. Dynamics of similar vortices: $\sigma < 1$

A qualitatively different behaviour appears for similar vortices. For $\sigma < 1$, the location-dependent potential becomes bi-variate (see figure 8), while the angle-dependent potential develops a double-welled shape (see figure 10 below). The requirement that the vortices cannot change sign restricts the physically relevant motion to the energy range $E > E_{s-}$.

For $E > E_{s-}$ both V_+ and V_- are defined in the range $(-y_e, y_e)$, but the dynamics is restricted to the regions $\pm(y_e, y_\pm)$ (see figures 4 and 8). As we can see from figure 9, the motion occurs consecutively in the two different potentials: the orbit follows the V_- potential from y_e to y_- and back, then it changes to V_+ and follows V_+ from y_e to y_+ and back, changes again to V_-, and so on (cf. figure 8). The mirror-image motion is also possible. Since the central hill of both branches is in the positive region, the centre of mass of the two vortices never crosses the $y = 0$ axis, and the motion is asymmetric. The net x-drift is negative. The centre of mass describes a semicircle-like half-loop, then it changes to another semicircle of different size, and repeats the two half-loop paths periodically. Whenever the orbit reaches $y = \pm y_e$, it becomes non-differentiable. In contrast to this "broken" centre-of-mass motion, the
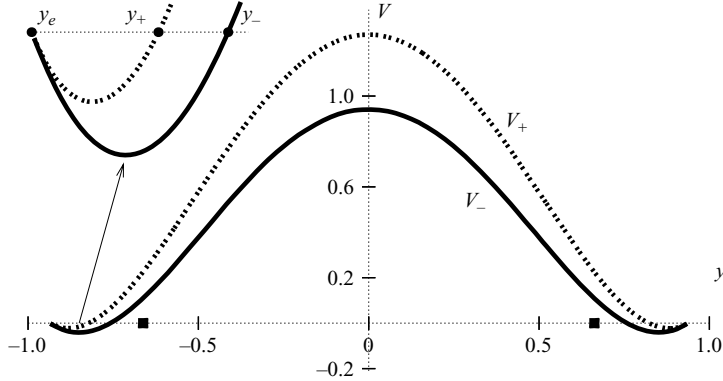
FIGURE 8. The location-dependent potential for similar vortices ($\sigma = 0.1$) for $E = 1.35$. The continuous and dashed lines represent V_- and V_+, respectively. Filled squares denote the values $\pm y_s$.
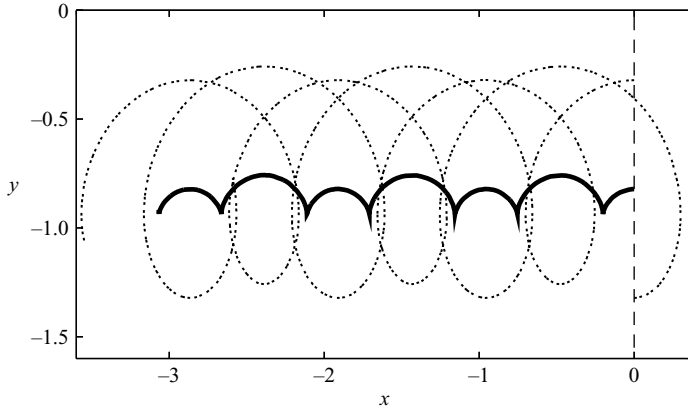

FIGURE 9. The "broken" path of the centre of mass of the two vortices (continuous line) and the path of the individual vortices (dashed lines). The parameters are the same as in figure 8, $\sigma = 0.1$, $\sigma' = 9.9$. Initial conditions: $\alpha_0 = 0$, $y_0 = -\sqrt{E/2} = -0.82$. $t_{sim} = 50$ dimensionless time units.

individual vortices smoothly loop around some point moving to the left (figure 9). The breaking of the orbit thus appears to be the consequence of constructing the mean value along the two smooth looping orbits of the vortices.

Since the energy is above the critical value E_c (see figure 10), a continuous overturning takes place in the angle dynamics.

7. Dynamics of sign-changing vortices
7.1. *Similar vortices $\sigma < 1$*

A change of the vortex sign occurs for energies $E_{min} < E < E_{s-}$. For rotational energy $E = E_{min} = -(\sigma - 1)^2/2$ of potential $W(\alpha)$ (see figure 10), only two angles – $\alpha = \pm \arccos(\sigma)$ – are accessible. The relative coordinate is then $y_r = -\sigma$. Since $\bar{y} = \sigma'/2$, then $y_1 = 1/\beta$, $y_2 = \kappa/\beta$: the strength of both vortices disappears
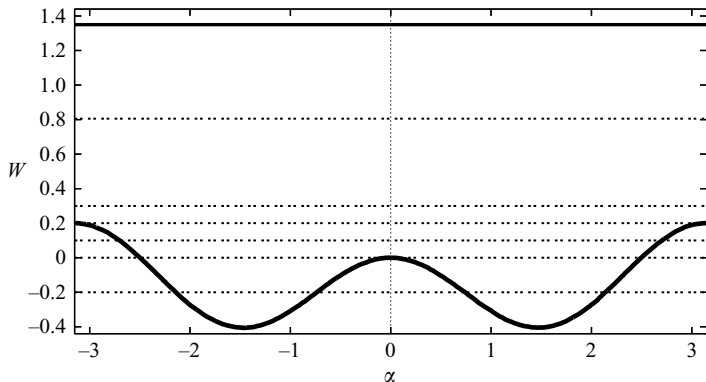
FIGURE 10. The angle-dependent potential $W(\alpha)$ ($\sigma = 0.1$, $\sigma' = 9.9$). The energies used in figures 9 and 11 are indicated as horizontal lines (continuous and dashed lines respectively).

(cf. (1.1)) and the centres stay at rest. For negative energies above E_{min}, two different finite intervals of angle become accessible. In this regime, both V_+ and V_- are negative, and therefore the motion extends to the full range $(-y_e, y_e)$. The orbit follows consecutively the two different branches of the location-dependent potential (figure 11a) and changes from one to the other at positions $\pm y_e$ (figure 12a).

At the value $E = 0$, a partial symmetry breaking takes place. The location-dependent potential V_+ touches the zero level. For any initial angle $\alpha_0 \neq 0$, orbits approach the straight line $y = 0$ asymptotically (figures 11b, 12b).

At larger energies, the motion in V_+ becomes restricted to one of the wells, whereas it remains extended in V_-: the centre of mass oscillates once between y_e, y_+ and y_e, there it changes to potential V_- and moves towards $-y_e$, where it changes to the other well of V_+, carries out an oscillation between the points $-y_e$ and $-y_+$, and switches back again to potential V_- (figure 11c). This cycle is repeated during the motion, giving birth to double-'broken' orbits (figure 12c).

At the energy value $E_c = 2\sigma$, another symmetry breaking takes place. This energy corresponds to the maximum of the angle-dependent potential W at $\alpha = \pi$ (see figure 10), meaning that an overturning of the vortices becomes possible. In the location-dependent potential, the middle hill of V_- touches the zero line (figure 11d). An orbit, starting at initial angle $\alpha_0 = 0$ (figure 12d) undergoes half an oscillation in the well of V_+, and then asymptotically approaches the $y = 0$ line.

For higher energies, the centre-of-mass motion is restricted to one side of the y-axis: it takes place in the intervals (y_-, y_e) or $(-y_e, -y_-)$ (see figures 11e,f, 12e,f). It is an interesting characteristic of the motion that singular spikes are now present in the individual vortex orbits also. These disappear as soon as the points $\pm y_s$ become the endpoints of the accessible y interval (cf. figure 12f).

7.2. *Significantly different vortices* $\sigma > 1$

A change of the vortex sign occurs for energies $E_{s+} < E < E_{s-}$. A typical trajectory can be seen in figure 13. The centre of mass and the stronger vortex exhibit a smooth looping around some points moving to the left, while the weaker vortex has a broken trajectory with periodically repeated spikes, like the ones found in the case of similar vortices.
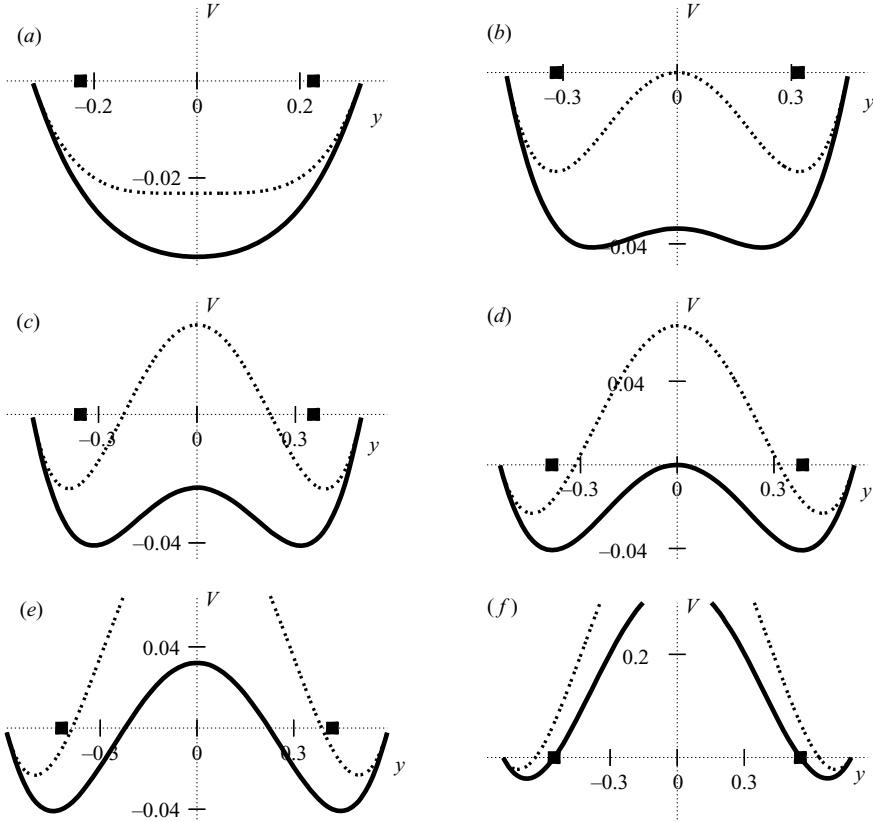
FIGURE 11. The location-dependent potential $V_\pm(y)$ corresponding to different energies for which sign change of the vortices is possible at the coordinates $\pm y_s$ (4.1), marked by filled squares. The continuous and dashed lines represent V_- and V_+, respectively. Here $\sigma = 0.1$, and $E_{min} = -0.405$, $E_{s-} = 0.805$. The energies are (a) $E = -0.2$, (b) $E = 0$, (c) $E = 0.1$, (d) $E = 0.2$, (e) $E = 0.3$, and (f) $E = 0.805$.

8. Advection in the field of the modulated vortices

In a frame co-moving with the modulated vortex couple, the flow field is time-periodic and, therefore, the advection dynamics is typically chaotic (Aref 1984; Ottino 1989; Velasco Fuentes *et al.* 1995). (An exception is the case of the critical energy E_c.) A feature of interest is the type of advective chaos.

Two basically different types of advective chaos have been identified: that taking place in closed containers (Aref 1984; Ottino 1989), and that generated by open flows (Jung *et al.* 1993; Péntek *et al.* 1995; Sommerer *et al.* 1996). In open flows there is a current flowing through the observation region to they have which particles, once escaped downstream, cannot return. The basic difference between the transport generated by closed and open flows is that particles remain trapped forever around the vortices in the first case, while they become transported in the far wake in the second case.

The advection dynamics is governed by the equation of motion

$$\dot{x} = -\frac{\partial \psi(x, y, t)}{\partial y}, \quad \dot{y} = \frac{\partial \psi(x, y, t)}{\partial x}. \tag{8.1}$$
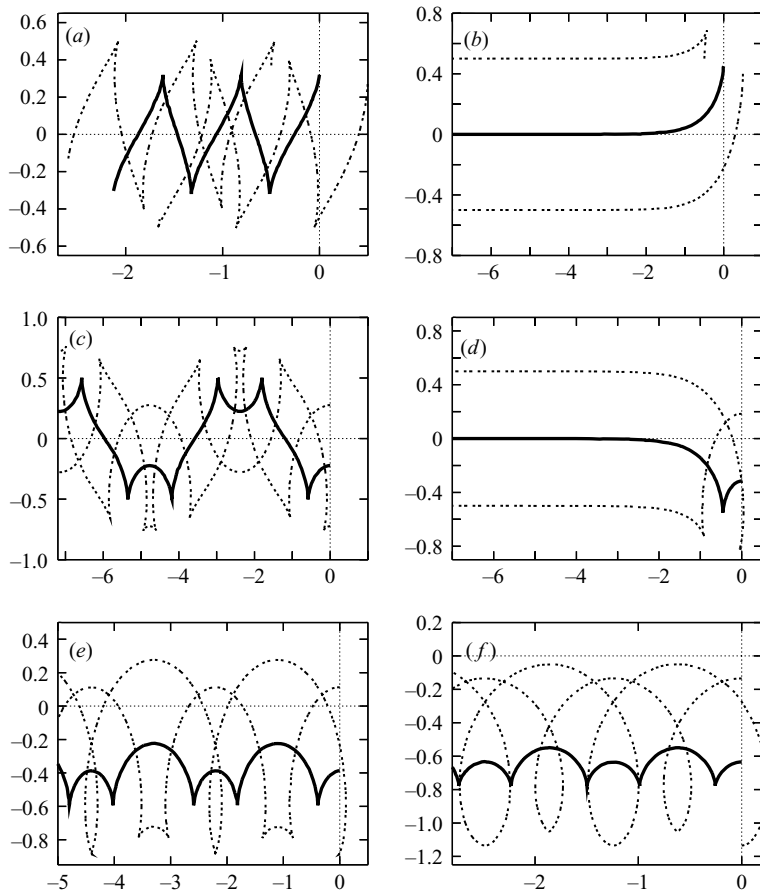
FIGURE 12. Vortex dynamics at the energies of figure 11. The continuous and dashed lines represent the orbit of the centre of mass and of the vortices, respectively. Parameters: $\sigma = 0.1$, $\sigma' = 9.9$ ($\kappa = 0.98$, $\beta = 0.2$). Initial conditions: (a, b) $\alpha_0 = \arccos(\sigma)$, $y_0 = \sqrt{(E - E_{min})/2}$; $(c\text{–}f)$ $\alpha_0 = 0$, $y_0 = \sqrt{E/2}$. The duration of simulation from (a) to (f) is $t_{sim} = 90, 83, 132, 73, 87$ and 57 dimensionless time units.
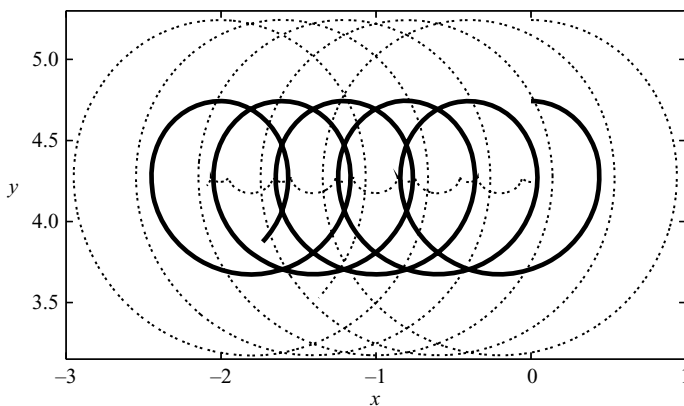

FIGURE 13. A plot similar to figure 9 but for $\sigma = 9$ at energy $E = 45$. $\sigma' = 1$. Initial conditions: $\alpha_0 = 0$, $y_0 = \sqrt{E/2} = 4.74$. $t_{sim} = 20$ dimensionless time units.

Here (x, y) denotes the location of the advected particle, and ψ the stream function. For the modulated point vortices

$$\psi(x, y, t) = -\sum_{i=1}^{2} \kappa_i(y_i(t)) \ln r_i(x, y, t), \qquad (8.2)$$

where $r_i(x, y, t) = \sqrt{(x - x_i(t))^2 + (y - y_i(t))^2}$ is the distance of the particle from the moving vortex centre i at time t.

The closed–open character of the flow can best be identified in a reference frame co-moving with the vortex centres. The origin is chosen to be the midpoint between vortices 1 and 2. If in this reference frame the points of a small droplet placed between the vortices at $t = 0$ remain distributed in a finite range around the vortices after arbitrarily long times, the flow is closed; otherwise it is open. Snapshots of the droplet are taken at integer multiples of the period of the vortex-dynamics. Since in our particular case the vortices start at initial angle $\alpha_0 = 0$, we define the period $T(E)$ of the flow as the time the vortices take to return to a position characterized by $\alpha = \alpha_0 = 0$. This period is different for each vortex orbit and it depends on the rotational energy, E, of the vortices.

We show that merely a change of the initial angle (the energy E) of the vortex centres can generate a switch between open and closed flow transport. A detailed quantitative study is presented for the case of significantly different vortices with $\sigma = 9$, but our arguments and the qualitative picture is valid for other vortex strength ratios as well.

The advection dynamics is clearly closed for high energies, $E > E_{s-}$, when both vortices are of the same sign over the entire motion. The points of a droplet initiated between the vortices never escape a circle of radius 2 (figure 14*a*). Some of these points become distributed between and around the vortices, while others move somewhat further away, surrounding four holes formed by KAM tori. Note that sufficiently close to each vortex there is a core, a region where the flow is very fast and impenetrable for particles coming from outside (a region also bounded by a KAM torus) (Péntek *et al.* 1995; Kuznetsov & Zaslavsky 1998, 2000; Leoncini, Kuznetsov & Zaslavsky 2001).

The region of small energies, $E < E_c$, clearly belongs to open advection since the total vortex strength vanishes whenever the centre-of-mass coordinate y vanishes. This implies the appearance of streamlines going out to infinity. Accordingly, points of a droplet lying outside the vortex core do escape any fixed region surrounding the vortices, and the droplet is distorted into a sequence of fractal lobes in the wake (see figure 14*b*). This open case is similar to the problem of Rom-Kedar, Leonard & Wiggins (1990), which also corresponds to a kind of modulated vortex pair, although modulation is there due to an external time-dependence.

The energy region $E_c < E < E_{s-}$ contains both types of advection dynamics with a cross-over between them. This cross-over energy is denoted by E_0 ($E_0 \approx 26$ for $\sigma = 9$), above which particles outside the vortex cores do not escape from the surroundings of the vortices over an observation time on the order of 50 periods. The passive advection is thus open in the entire range $E < E_0$ (figure 15*a*).

The topology of the lobe structures changes when the energy of the system crosses the critical energy E_c. In figure 14(*b*) (below E_c) the vortices extend over both wells of potential V. Since the vortex orbit crosses the $\bar{y} = \sigma'/2$ level, which represents an axis of symmetry for the vortex motion (figure 5*d*), in the advection dynamics lobes are formed both in the positive and negative y-direction, consecutively. In figure 15(*a*) (above E_c) the vortex motion is restricted to one well of the potential V and the
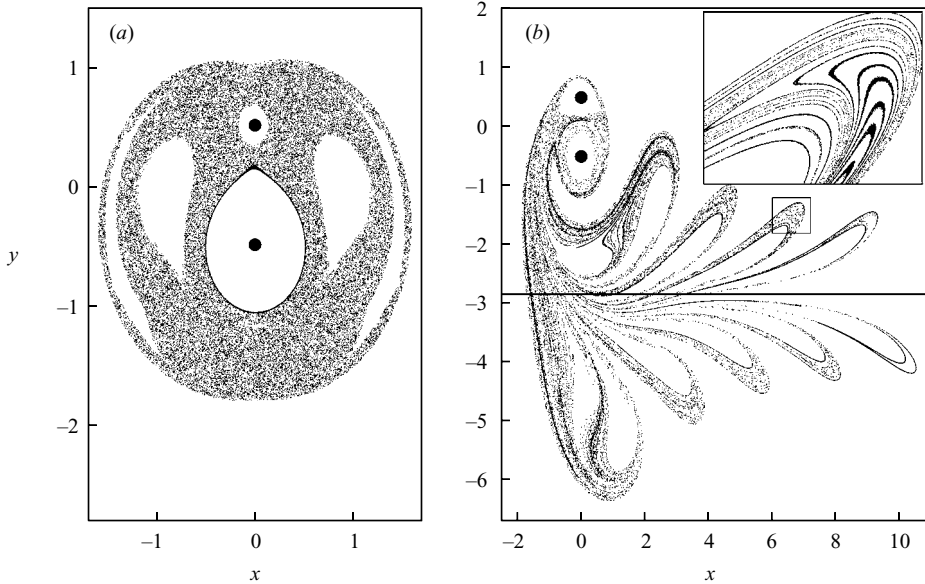
FIGURE 14. Particle advection. (*a*) Closed dynamics $E = 100 > E_{s-}$, $\sigma = 9$. Shape of a droplet of size 200×200 points initiated at $[-0.1, 0.1] \times [0.13, 0.23]$ after 50 periods T of the vortex dynamics, where $T(E = 100) = 1.165$ time units. (*b*) Open dynamics, $E = 16 < E_c$, $\sigma = 9$. Shape of a droplet of size 300×300 points initiated in $[-0.1, 0.1] \times [0.07, 0.17]$ after 5 periods of the vortices, where $T(E = 16) = 8.365$ time units. The horizontal line represents $\bar{y} = \sigma'/2$, the symmetry axis of the location-dependent potential (see (2.11)). The vortex centres are denoted by black dots. Inset: magnification of the small square in panel (*b*).

symmetry of the trajectories disappears (figure 5*f*). Accordingly, advected particles in such cases form lobes only in one direction.

From a dynamical systems point of view, the basic difference between closed and open cases lies in the structure of the chaotic set. For closed chaotic advection, which is an example of closed Hamiltonian chaos, the chaotic set extends over a two-dimensional area of the fluid surface. The region filled in asymptotically by the droplet points (see figure 14*a*) is part of the chaotic set, and other such areas might also exist, reachable from other initial droplet positions. In contrast, the chaotic invariant set of the open advection dynamics contains fractal parts of zero area (figure 15*b*). This chaotic saddle (Jung *et al.* 1993; Péntek *et al.* 1995; Tél & Gruiz 2006) is formed by an infinity of unstable particle orbits which are trapped by the vortices forever, both forward and backward in time. In such cases points of a droplet come close to the chaotic saddle, but leave it sooner or later. Their asymptotic form is determined by the unstable manifold (Jung *et al.* 1993; Péntek *et al.* 1995), itself a fractal, of the chaotic saddle.

In the open range $E < E_0$, a special case is the figure-of-eight-shaped orbit, as first pointed out in Velasco Fuentes & van Heijst (1994). Since the orbit is closed, the vortices repeatedly re-enter the wake, and thus produce an advection which is only transiently open (figure 16*a*). The droplet points later become distributed in a large but finite area (figure 16*b*), indicating that the asymptotic advection dynamics is closed. One can observe a very slow expansion of the chaotic set even at late times.

A statistical measure of the strength of the Lagrangian transport out of the neighbourhood of the vortices is provided by the escape rate (Tél & Gruiz 2006).
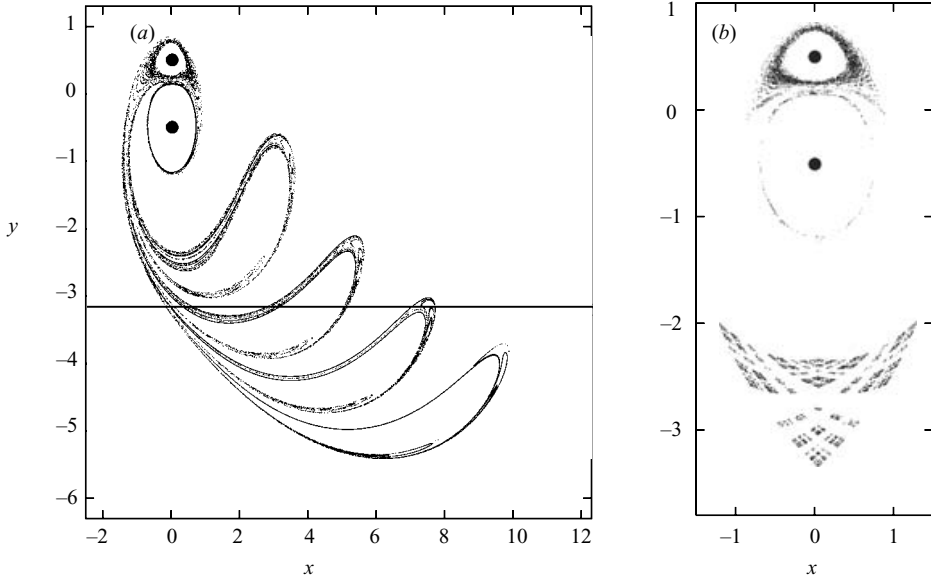
FIGURE 15. Open advection for $E_c < E = 20 < E_0$. (a) Shape of a droplet of size 300×300 points initiated at $[-0.1, 0.1] \times [0.13, 0.23]$ after $5T$, where $T(E = 20) = 4.017$ time units. The horizontal line again represents the level $\bar{y} = \sigma'/2$. (b) The chaotic invariant set (a chaotic saddle) obtained by starting 4×10^6 points in $[-1.5, 1.5] \times [-3.5, 1.5]$ and plotting at $5T$ the positions of those points which do not escape the wake (do not cross the $x = 6$ line) up to $20T$ as in Benczik, Tél & Toroczkai (2003). The set turns out to contain points around the vortex cores as well, where the set appears to be dense.
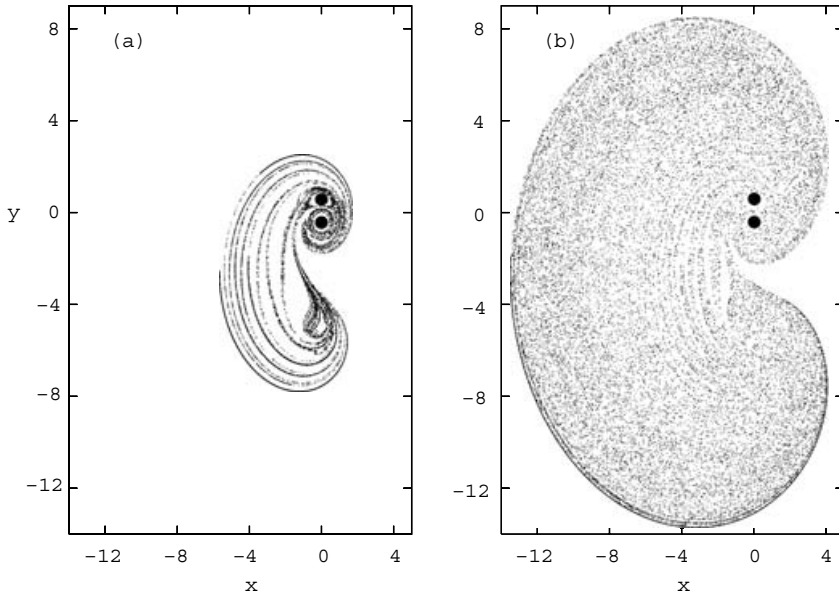

FIGURE 16. Transiently open advection dynamics of the figure-of-eight orbit, $E = E_8 = 14.2746 < E_c$, $\sigma = 9$. Shape of a droplet of size 300×300 points initiated at $[-0.1, 0.1] \times [0.07, 0.17]$ after (a) $5T$, (b) $50T$, where $T(E_8) = 7.483$ time units.
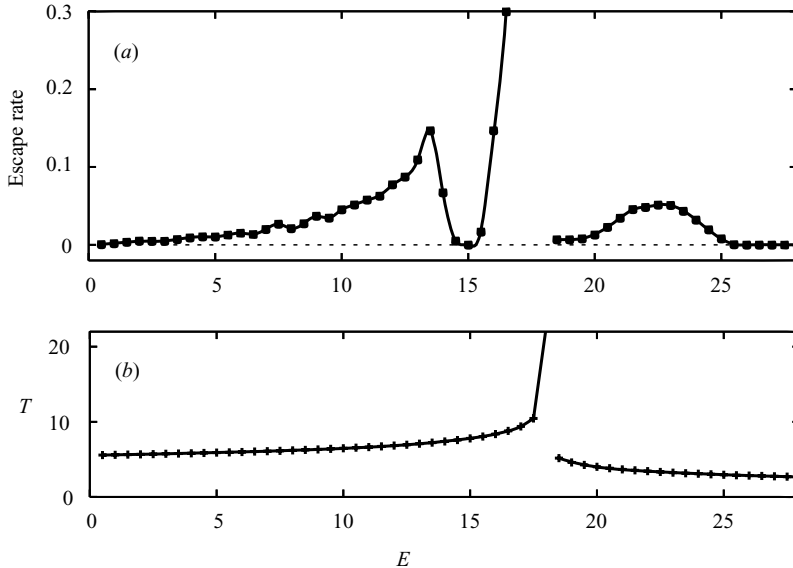
FIGURE 17. (*a*) Dependence of the escape rate kT over a period T on the energy E of the vortex couple for $\sigma = 9$. We started 250 000 uniformly distributed particles in a circle of radius 1 around the centre of mass of the vortices, and measured the number $N(t = nT)$ of non-escaped particles at integer multiples n of the vortex period $T(E)$. A particle was considered to have escaped if it left a square of size 16×16 centred at the centre of mass. Particles in the vortex cores, i.e. in a circle of radius 0.47 around the individual vortices, are excluded from the statistics. To determine kT we took the average slope of the function $\ln N$ versus n in the interval $n \in (10, 20)$ since the very long-time behaviour is typically dominated by a non-exponential decay due to KAM tori. (*b*) The period T of the vortex motion as a function of energy E.

We start with a large number of particles distributed in a fixed region around the vortices. The escape from the chaotic set of open flows is known to be exponential, i.e. the number of non-escaped particles after time t is proportional to $\exp(-kt)$, where k is the escape rate. The escape rate of particles starting outside the vortex cores (or other KAM tori) is independent of the region chosen for the initial conditions; it is thus a property of the chaotic saddle (Tél & Gruiz 2006). In figure 17(*a*) we display the escape rate $kT(E)$ over a period of the flow. One can see that the escape process takes place faster and faster with increasing energies, until the couple approaches the energy of the figure-of-eight orbit. The vanishing escape rate at this energy shows that the flow is only transiently open; the particles of the droplet eventually become trapped around the vortices. Increasing the energy further, the escape rate kT formally develops a singularity at the critical energy E_c since at this point the period of the vortex motion is infinite (see figure 17*b*). In the region $E_c < E < E_0$ the flow is still open, and consequently the escape rate is non-zero. Finally, the vanishing escape rate at energy E_0 represents the transition from an open to closed flow regime. For higher energies, all the particles are trapped around the vortices forever.

9. Conclusions

We have shown that a linearly location-dependent modulation of the vortex strength, modelling the β-effect, leads to a complex, though integrable, motion of a couple of vortices. This dynamics can best be described in terms of effective potentials.

To understand the complete dynamics of the modulated point vortices we need information from two potentials: the angle dynamics can be extracted from potential $W(\alpha)$, while potential $V(y)$ provides information about the spatial shape. From the point of view of the centre-of-mass orbits, the location-dependent potential V contains much more information than the angle-dependent potential, and it has the unusual feature of bi-valuedness in a broad range of parameters. As a consequence, the centre-of-mass orbit develops spikes in such cases. It is also possible to deduce two other potentials $V_1(y_1)$ and $V_2(y_2)$ describing the motion of the individual vortices 1 and 2, respectively. The full information provided by the two new potentials V_1 and V_2 gives a full description of the global dynamics, equivalent to the representation by potentials V and W.

The β-effect makes the advection dynamics chaotic in the field of the two modulated vortices. An interesting feature found here is the change in the character of the advection process due to a change in the initial condition of the couple. The initial angle determines whether the vortices are able to trap an area of the fluid in their neighbourhood (outside the cores or other tori) forever, or whether they can only generate transient stirring, and eventually leave all the advected particles (with the exception of a small set) in their wake.

Finally, we point out an interesting analogy between the dynamics of a modulated point-vortex couple and that of a single inertial orbit on a rotating Earth worked out by Paldor and coworkers (Paldor & Killworth 1988; Paldor & Boss 1992; Rom-Kedar, Dvorkin & Paldor 1997; Dvorkin & Paldor 1999; Paldor 2007). The orbits of figure 5 are remarkably similar to the ones shown in figure 1 of Paldor & Killworth (1988), indicating that a typical centre-of-mass orbit of the vortex couple is similar to that of a point mass, although the latter is on a rotating sphere where the latitude-dependence of the Coriolis parameter is taken into account without any approximation. Mathematically, the explanation lies in the similarity of the equations of motion: both take place in a potential whose shape changes from single-welled to double-welled. Physically, the reason is that the vortex couple is a kind of rotator, with the rotation angle as an internal degree of freedom (the distance between the vortices is fixed), but the centre of mass, subjected to the β-effect, can exhibit similar motion to a single point mass.

Appendix. The figure-of-eight-shaped orbit

The appearance of a figure-of-eight orbit and the sign change of the drift is not accompanied by any characteristic change of the potentials W or V. This is due to the fact that the equation of motion for the centre-of-mass coordinate x is decoupled from that of the other degrees of freedom. From (2.13) and (3.1) the drift velocity along the x-axis is, in terms of the rotational angle,

$$\frac{\mathrm{d}x}{\mathrm{d}t} = \frac{\beta}{2}(\sigma - \cos\alpha)\cos\alpha. \tag{A 1}$$

For periodic dynamics, the average drift velocity is

$$\overline{v} = \frac{\beta}{2}\overline{(\sigma - \cos\alpha)\cos\alpha}, \tag{A 2}$$

where the averaging is taken over a single time period $T(E)$. Owing to the nonlinearity of the problem, no exact statement can be made, but a perturbation theory can successfully be applied.

Let us consider the equation of motion for the angle around the origin, expanded up to third order in α, for $\sigma > 1$. From (3.3)

$$\frac{\mathrm{d}^2\alpha}{\mathrm{d}t^2} = -\beta^2(\sigma - 1)\alpha + \beta^2\frac{\sigma - 4}{6}\alpha^3. \tag{A 3}$$

The perturbation solution of this nonlinear oscillator dynamics with initial angle α_0 and zero initial angular velocity is known to be (see e.g. Landau & Lifshitz 1985)

$$\alpha(t) = \alpha_0 \cos\omega t - \frac{\alpha_0^3(\sigma - 4)}{192(\sigma - 1)}\cos 3\omega t \tag{A 4}$$

with frequency

$$\omega = \beta\sqrt{\sigma - 1}\left(1 - \frac{\sigma - 4}{16(\sigma - 1)}\alpha_0^2\right). \tag{A 5}$$

The average drift velocity from (A 2) is at second non-trivial order

$$\bar{v} = \frac{\beta}{2}\left(\sigma - 1 - \frac{\sigma - 2}{2}\overline{\alpha^2} + \frac{\sigma - 8}{24}\overline{\alpha^4}\right). \tag{A 6}$$

Since $\alpha(t)$ can be expressed by cosine functions,

$$\overline{\alpha^2} = \tfrac{1}{2}\alpha_0^2, \quad \overline{\alpha^4} = \tfrac{3}{8}\alpha_0^4. \tag{A 7}$$

The initial angle is related to the energy E:

$$E = W(\alpha_0) = \frac{\sigma - 1}{2}\alpha_0^2 - \frac{\sigma - 4}{24}\alpha_0^4, \tag{A 8}$$

from which

$$\alpha_0^2 = \frac{2}{\sigma - 1}E + \frac{\sigma - 4}{3(\sigma - 1)^3}E^2. \tag{A 9}$$

The average drift velocity is thus expressed in terms of the energy as

$$\bar{v} = \frac{\beta}{2}\left(\sigma - 1 - \frac{\sigma - 2}{2(\sigma - 1)}E - \frac{\sigma^2 + 3\sigma + 8}{48(\sigma - 1)^3}E^2\right). \tag{A 10}$$

The wavelength of the orbit is then $\lambda = \bar{v}2\pi/\omega$ with the frequency given by (A 5).

From the vanishing of the drift velocity we obtain the perturbative result for the energy value E_8 of the figure-of-eight orbit

$$E_8 = \frac{2(\sigma - 1)^2}{\sigma - 2}\left(1 - \frac{\sigma^2 + 3\sigma + 8}{12(\sigma - 2)^2}\right). \tag{A 11}$$

For $\sigma = 9$ used in figure 5 this first-order approximation yields $E_8 = 14.678$.

REFERENCES

AREF, H. 1984 *J. Fluid Mech.* **143**, 1.

AREF, H. 2002 *Phys. Fluids* **14**, 1315.

BENCZIK, I. J., TOROCZKAI, Z. & TÉL, T. 2003 *Phys. Rev. E* **67**, 036303.

DVORKIN, Y. & PALDOR, N. J. 1999 *Atmos Sci.* **56**, 1229.

HOBSON, D. D. 1991 *Phys. Fluids A* **3**, 3027.

JAMALOODEEN, M. I. & NEWTON, P. 2006 *Proc. R. Soc. Lond. A* **462**, 3277–3299.

JUNG, C., TÉL, T. & ZIEMNIAK, E. 1993 *Chaos* **3**, 555.

KLOOSTERZIEL, R. C., CARNEVALE, G. F. & PHILIPPE, D. 1993 *Dyn. Atmos. Oceans* **19**, 65.

KUZNETSOV, L. & ZASLAVSKY, G. M. 1998 *Phys. Rev.* E **58**, 7330.

KUZNETSOV, L. & ZASLAVSKY, G. M. 2000 *Phys. Rev.* E **61**, 3772.

LANDAU, L. D. & LIFSHITZ, E. N. 1985 *Classical Mechanics.* Pergamon.

LEONCINI, X., KUZNETSOV, L. & ZASLAVSKY, G. M. 2001 *Phys. Rev.* E **63**, 036224.

MAKINO, M., KAMIMURA, T. & TANIUTI, T. 1981 *J. Phys. Soc. Japan* **50**, 980.

NEWTON, P. 2001 *The N-vortex Problem: Analytical Techniques.* Springer.

NEWTON, P. & SHOKRANEH, H. 2006 *Proc. R. Soc. Lond.* A **462**, 149.

OTTINO, J. M. 1989 *The Kinematics of Mixing: Stretching, Chaos & Transport.* Cambridge University Press.

PALDOR, N. 2007 In *Lagrangian Analysis and Prediction of Coastal and Ocean Dynamics* (ed. A Griffa, A. D. Kirwan, A. J. Marino, T. Özgökimen & T. Rossby), pp. 119–135. Cambridge University Press.

PALDOR, N. & BOSS, E. 1992 *J. Atmos. Sci.* **49**, 2306.

PALDOR, N. & KILLWORTH, P. D. 1988 *J. Atmos. Sci.* **45**, 4013.

PEDLOSKY, J. 1979 *Geophysical Fluid Dynamics.* Springer.

PÉNTEK, Á., TÉL, T. & TOROCZKAI, Z. 1995 *J. Phys.* A **28**, 2191.

ROM-KEDAR, V., DVORKIN, Y. & PALDOR, N. 1997 *Physica* D **106**, 389.

ROM-KEDAR, V., LEONARD, A. & WIGGINS, S. 1990 *J. Fluid Mech.* **214**, 347.

SOMMERER, J. C., KU, H.-C. & GILREATH, H. E. 1996 *Phys. Rev. Lett.* **77**, 5055.

TÉL, T. & GRUIZ, M. 2006 *Chaotic Dynamics.* Cambridge University Press.

VELASCO FUENTES, O. U. & VAN HEIJST, G. J. F. 1994 *J. Fluid Mech.* **259**, 79.

VELASCO FUENTES, O. U. & VAN HEIJST, G. J. F. 1995 *Phys. Fluids* **7**, 2735.

VELASCO FUENTES, O. U., VAN HEIJST, G. J. F. & CREMERS, B. E. 1995 *J. Fluid Mech.* **291**, 139.

VELASCO FUENTES, O.U. & VELÁZQUES MŨNOZ, F. A. 2003 *Phys. Fluids* **15**, 1021.

ZABUSKY, N. J. & MCWILLIAMS, J. C. 1982 *Phys. Fluids* **25**, 2175.